THE ASTROPHYSICAL JOURNAL SUPPLEMENT SERIES, 112:271–283, 1997 October

STEPS TOWARD DETERMINATION OF THE SIZE AND STRUCTURE OF THE BROAD-LINE REGION IN ACTIVE GALACTIC NUCLEI. X. VARIABILITY OF FAIRALL 9 FROM OPTICAL DATA[1]

M. SANTOS-LLEÓ,[2] E. CHATZICHRISTOU,[3] C. MENDES DE OLIVEIRA,[4] C. WINGE,[5,6] D. ALLOIN,[7] B. M. PETERSON,[8] P. M. RODRÍGUEZ-PASCUAL,[9] G. M. STIRPE,[10] T. BEERS,[11] A. BRAGAGLIA,[10] J.-F. CLAESKENS,[12] M. FEDERSPIEL,[13] E. GIANNUZZO,[14] J. GREGORIO-HETEM,[4] G. MATHYS,[15] I. SALAMANCA,[16] P. STEIN,[17] B. STENHOLM,[18] R. WILHELM,[19] C. ZANIN,[20] P. ALBRECHT,[21] J. CALDERÓN,[22] C. A. CARETTA,[23,6] G. CARRANZA,[22] R. D. D. DA COSTA,[4] R. DIAZ,[22] M. DIETRICH,[24] H. DOTTORI,[5] F. ELIZALDE,[25,6] G. GOLDES,[22] K. K. GHOSH,[26] M. A. G. MAIA,[23,6] S. PAOLANTONIO,[22] I. RODRIGUES DE OLIVEIRA FILHO,[5,6] A. RODRIGUEZ-ARDILA,[5,6] H. R. SCHMITT,[5,6] S. SOUNDARARAJAPERUMAL,[26] R. E. DE SOUZA,[4] C. N. A. WILLMER,[23,6] AND W. ZHENG[27]

Received 1997 February 27; accepted 1997 April 15

ABSTRACT

The results of an optical monitoring campaign on the active nucleus in the luminous Seyfert 1 galaxy Fairall 9 are presented. This campaign was undertaken in parallel with ultraviolet spectroscopic monitoring with the *IUE* satellite which is described in a separate paper. The primary purpose of this program is to measure the response times (or "lags") of the emission lines to continuum variations and thus to extend the range in luminosity of active galactic nuclei (AGNs) for which such measurements have been made. The main conclusions of this work are as follows:

1. Continuum (at 5340 Å) variations of amplitude $\sim 12\%$ are detected on timescales as short as ~ 20 days. These variations are much larger than the typical uncertainties in the measurements, which are of order $\sim 2\%$. Over ~ 94 days, a factor of 2 change in the *nuclear* continuum was observed.

2. The optical continuum light curve resembles that of the UV continuum, showing two "events" of low-amplitude variations with a duration of ~ 70 days and with no measurable lag between the UV and optical continuum light curves. The UV data show a third larger amplitude event that occurred after the optical monitoring had terminated and unfortunately went unobserved in the optical.

3. The Hβ emission-line flux also underwent significant, low-amplitude ($\geq 20\%$) variations. Cross-correlation analysis reveals that Hβ lags behind the UV continuum by about 23 days, a value much smaller than what was previously suggested by earlier variability studies. However, this small lag is consistent with the lags for the UV lines during this campaign in the sense that the Hβ lag is approximately 50% larger than that of Lyα λ1216, as it has been found for lower luminosity AGNs.

4. The Hβ difference profile produced by subtracting the low-state from the high-state data can be described as a two-component structure with blue and red components of similar width (~ 2500 km s^{-1}) and that appear to vary in phase.

Subject headings: galaxies: active — galaxies: individual (Fairall 9) — galaxies: nuclei — galaxies: Seyfert

[1] Partly based on observations collected at the European Southern Observatory, La Silla, Chile and at the Observatório do Pico dos Dias, Minas Gerais, Brazil.

[2] Laboratorio Astrofisica Espacial y Física Fundamental, LAEFF-INTA, Apartado 50727, Madrid, Spain.
[3] Sterrewacht Leiden, Postbus 9513, 2300 R.A. Leiden, Netherlands.
[4] Universidade de São Paulo, C.P. 9638, 01065-970 São Paulo, Brazil.
[5] Departamento de Astronomia, Instituto de Física, Universidade Federal do Rio Grande do Sul, Avenida Bento Gonçalves, 9500, CP15051, CEP 91500, Porto Alegre, RS, Brazil.
[6] CNPq Fellow.
[7] URA CNRS D2052, Service d'Astrophysique, CE Saclay, 91191 Gif sur Yvette, France.
[8] Department of Astronomy, Ohio State University, 174 West 18th Avenue, Columbus, OH 43210.
[9] ESA IUE Observatory, P.O. Box 50727, 28080 Madrid, Spain.
[10] Osservatorio Astronomico di Bologna, Via Zamboni 33, I-40126, Bologna, Italy.
[11] Department of Physics and Astronomy, Michigan State University, East Lansing, MI 48824,
[12] Institut d'Astrophysique, Université de Liège, Av. de Cointe 5, B-4000 Liège, Belgium.
[13] Astronomisches Institut, Universitaet Basel, Venusstrase 7, CH-4102 Binningen, Switzerland.
[14] Dipartamento di Astronomia, Universitá degli Studi di Bologna, Via Zamboni 33, I-40126, Bologna, Italy.
[15] ESO, Casilla 19001, Santiago 19, Chile.
[16] Royal Greenwich Observatory, Madingley Road, Cambridge CB3 0HA, United Kingdom.
[17] Departament d'Astronomia i Meteorologia, Universitat de Barcelona, Avenida Diagonal 647, Barcelona, Spain.
[18] Lund Observatory, BOX 43, S-22100 Lund, Sweden.
[19] McDonald Observatory, RLM 15.308, University of Texas, Austin, TX 78712.
[20] Institut für Astronomie, Universität Innsbruck, Technikerstrasse 25, A-6020 Innsbruck, Austria.
[21] Universitäts-Sternwarte Göttingen, Geismarlandstrasse 11, D-37083 Göttingen, Germany.
[22] Observatorio Astronómico de Córdoba, Laprida 854, 5000 Córdoba, Argentina.
[23] Departamento de Astronomia, Observatório Nacional, Rua Gal. José Cristino 77, CEP 20921-030 Rio de Janeiro, RJ, Brazil.
[24] Landessternwarte Heidelberg, Königstuhl, D-69117 Heidelberg, Germany.
[25] Divisão de Astrofisica, Instituto Nacional de Pesquisas Espaciais, C.P. 515, CEP 12201-970, São José dos Campos, SP, Brazil.
[26] Vainu Bappu Observatory, Indian Institute of Astrophysics, Kavalur, Alangayam 635701, Tamil Nadu, India.
[27] Department of Physics and Astronomy, The Johns Hopkins University, Baltimore, MD 21218.

1. INTRODUCTION

The continuum source and the broad-line region (BLR) in active galactic nuclei (AGNs) are far too small to be resolved spatially even with diffraction-limited 10 m class telescopes. Consequently, much of what is known about the small-scale (i.e., parsec or less) structure is based on studies of continuum and emission-line variability. Since the late 1980s in particular, attempts have been made to make use of coordinated continuum and emission-line variations to determine the structure and kinematics of the BLR through "reverberation mapping" (Blandford & McKee 1982). Early spectroscopic monitoring programs on AGNs (see Peterson 1988 for a review) made it clear that while emission-line and continuum variability afforded a potentially powerful tool to probe the inner structure of AGNs, very massive observational efforts would be required to do this effectively. This led to the formation of large consortia to carry out multiwavelength spectroscopic monitoring programs on AGNs. This paper describes recent work by the largest of these consortia, the International AGN Watch (Alloin et al. 1994), on the high-luminosity Seyfert 1 galaxy Fairall 9 ($-24 < M_V \leq -23$). This program was undertaken in support of a concurrent UV monitoring program carried out with the *International Ultraviolet Explorer* (*IUE*), which is described in a separate contribution (Rodríguez-Pascual et al. 1997; hereafter Paper IX), which also includes a brief up-to-date summary of published work by the International AGN Watch. As explained in Paper IX, the luminosity range for which these results have been obtained is $10^{39} \lesssim L_\lambda(1450\ \text{Å}) \lesssim 10^{40}$ ergs s^{-1} Å^{-1} and extension of variability studies to higher luminosities is highly desirable.

Fairall 9 (F9) is a southern hemisphere galaxy, at a redshift $z = 0.0461$. It has previously been extensively studied at many wavelengths, as most recently summarized by Recondo-González et al. (1997). It has undergone the most dramatic variations ever observed in nonblazar AGNs; between 1978 and 1984, the UV continuum flux decreased by a factor of 30. Since 1984, it has continued to vary, but with an amplitude more characteristic of mean-luminosity Seyfert 1 galaxies (i.e., over a factor of 2–3). Even in the lower luminosity state that it has been in since the mid-1980s, F9 is still among the most luminous Seyfert 1 galaxies, with UV luminosities above the upper limit of the previous (already observed) luminosity range [at present $L_\lambda(1450\ \text{Å}) > 10^{41}$ ergs s^{-1} Å^{-1}, while its historical maximum is $L_\lambda(1450\ \text{Å}) \sim 2.2 \times 10^{42}$ ergs s^{-1} Å^{-1}, assuming $H_0 = 75\ \text{km s}^{-1}\ \text{Mpc}^{-1}$].

As described in Paper IX, a UV spectroscopic monitoring program on F9 was undertaken with the primary goal of extending well-sampled variability studies to high-luminosity Seyfert galaxies. The specific reasons for carrying out a contemporaneous ground-based optical campaign are as follows:

1. To test whether variations on short timescales (days to weeks) are superimposed on the long-term changes already known to occur in F9. This would provide clues about the physical origin of the variations of the continuum.

2. To check whether the UV and optical continua vary simultaneously, as has been found for lower luminosity Seyfert galaxies. This is particularly important in this case (*a*) since it is no longer possible to obtain reliable optical fluxes with the Fine Error Sensor (FES) on *IUE* and mainly (*b*) since in the standard thin accretion disk model, the separation between the regions in the disk that produce the bulk of the UV and of the optical continua is larger for the higher luminosity objects, and thus measurement of any time delay between the UV and optical variations should be easier.

3. To measure the time lags τ between the optical-line (principally Hβ) and continuum variations, which gives an indication of the size of the line-emitting region $R \approx c\tau$. This has not been done before in the case of F9 for variations with typical timescales similar to or less than a few months, although emission-line variability with this timescale has been detected (see, e.g., Winge et al. 1996). With accurate determination of τ, it is possible to check the naive theoretical prediction that $R \propto L^{1/2}$, where L is the AGN continuum luminosity (see Peterson 1993). Comparison of the time lags of the optical lines with those for the UV lines is important to determine whether or not there is evidence for radial ionization stratification of the BLR, as has been inferred for lower luminosity Seyfert galaxies.

4. To look for profile variability of the Hβ emission line in order to put constraints on the kinematical models of the BLR.

This paper presents the results of the optical monitoring campaign on Fairall 9 and compares them with those obtained in the UV as described in Paper IX. The observations and data analysis are described in § 2. In §§ 3 and 4, the optical continuum and Hβ light curves are presented. The pattern of variability of the continuum, Hβ total intensity variations, and the Hβ emission-line profile are analyzed in § 5. The results are summarized and discussed in § 6.

2. OBSERVATIONS

2.1. *Data and Reduction*

Regular spectroscopic observations of the active nucleus of Fairall 9 were scheduled once every 4 days between 1994 May 3 and September 28 on the European Southern Observatory (ESO) 1.5 m telescope with the Boller & Chivens spectrograph and a CCD detector. There are a few missing epochs, however: two of them are due to a large block of time scheduled with an instrument that was not suitable for faint-object observations, and the rest are due to poor weather conditions. The detailed set-up was not uniform because this program was sharing nights with other programs, as this program required only 2.5 hr per night. In addition to this regularly scheduled time, some additional observations were also made by individual observers on the 1.5 m ESO telescope. Altogether, spectra for 29 epochs were obtained between 1994 May 3 and November 1. Table 1 shows a journal of the observations, including those from other sources as described below. The first two columns give the Julian and civil dates of the midpoint of the observation, and the third column gives a code referring to the origin of the data (telescope and site). Also given are the effective air mass, projected aperture geometry (slit width times extracted length in the spatial direction, in seconds of arc), nominal resolution, spectral range, total integration time, and additional comments referring to the photometric

TABLE 1

JOURNAL OF SPECTROSCOPIC OBSERVATIONS

JD (−2,449,000) (1)	UT Date (2)	Data Origin[a] (3)	Air Mass (4)	Aperture (arcsec) (5)	Resolution Å (6)	Range Å (7)	Integration Time (s) (8)	Notes[b] (9)
475.924	1994 May 3	E	1.97	4 × 9	4.3	4410–6400	1200	
479.930	1994 May 7	E	1.81	4 × 9	4.3	4410–6400	1500	
483.933	1994 May 11	E	1.75	4 × 9	4.2	4500–6500	2700	
487.922	1994 May 15	E	1.76	4 × 9	10	4000–7880	3000	1
491.924	1994 May 19	E	1.67	4 × 9	3.15	4320–5600	3600	1
491.937	1994 May 19	C	1.38	6 × 10	8.9	4639–6069	3600	
499.909	1994 May 27	E	1.65	4 × 9	1.2	4600–5650	3600	2
511.930	1994 Jun 8	E	1.35	4 × 9	4.2	4100–6100	3600	
514.846	1994 Jun 11	L	1.47	6 × 8	12	4200–7900	3600	
515.832	1994 Jun 12	L	1.52	6 × 10	12	4200–7900	3300	
515.904	1994 Jun 12	E	1.43	4 × 9	4.2	4100–5900	3600	
519.932	1994 Jun 16	E	1.31	4 × 9	10	3980–7848	4200	3
523.929	1994 Jun 20	E	1.28	4 × 9	4.2	4610–6590	4200	
531.918	1994 Jun 28	E	1.25	4 × 9	16	3475–9145	4200	
535.919	1994 Jul 2	E	1.23	4 × 9	21	3000–5650	4200	1
539.883	1994 Jul 6	E	1.23	4 × 9	10	4200–7400	1200	
542.906	1994 Jul 9	C	1.17	7.2 × 9.2	15	3737–6687	1800	4
543.832	1994 Jul 10	L	2.04	6 × 15	12	3752–8466	1200	5
543.883	1994 Jul 10	C	1.20	7.2 × 9.2	15	4404–7165	1800	4
543.900	1994 Jul 10	E	1.21	4 × 9	10	3700–6400	3600	1
544.918	1994 Jul 11	C2	1.13	7.2 × 8.5	11	3782–7112	1200	4
545.799	1994 Jul 12	L	1.50	6 × 10	12	4200–7900	6000	
547.908	1994 Jul 14	E	1.18	4 × 9	16	3320–9020	3600	3
547.924	1994 Jul 14	C	1.13	5 × 10.5	11	4102–6894	900	
554.826	1994 Jul 21	L	1.25	3 × 12	12	4200–7900	3600	
555.910	1994 Jul 22	E	1.16	4 × 9	10	3545–5475	3780	6
559.905	1994 Jul 26	E	1.16	4 × 9	10	3545–6400	3900	1
567.884	1994 Aug 3	E	1.16	4 × 9	6.3	4490–6400	3600	1
575.861	1994 Aug 11	E	1.16	4 × 9	16	3560–6400	3600	1
576.925	1994 Aug 12	E2	1.19	2 × 6.7	10	3761–6938	600	1
579.852	1994 Aug 15	E	1.16	4 × 9	16	3560–6400	5400	
591.809	1994 Aug 27	E	1.16	4 × 9	10	3827–7764	3600	3
595.776	1994 Aug 31	E	1.18	4 × 9	6.3	4490–7124	3600	
599.736	1994 Sep 4	E	1.16	4 × 9	6.3	4490–6630	3600	
599.740	1994 Sep 4	L	1.24	5 × 10	13	3500–7500	2400	7
607.731	1994 Sep 12	E	1.20	4 × 9	21	4400–10330	3900	
619.733	1994 Sep 24	E	1.16	4 × 9	16	3600–8500	3600	3
623.725	1994 Sep 28	E	1.18	4 × 9	10	3520–6600	3600	
625.694	1994 Sep 30	L	1.26	6 × 40	16	3630–8314	1800	7
626.676	1994 Oct 1	E	1.15	4 × 9	10	3520–6600	3600	
628.733	1994 Oct 3	L	1.34	6 × 12	14	4080–8315	1800	7
653.739	1994 Oct 28	E	1.24	4 × 9	6.3	4490–7120	3000	
664.676	1994 Nov 8	E	1.18	4 × 9	10	4450–8450	3600	
724.604	1995 Jan 7	E2	1.43	1.5 × 5	10	4000–6935	180	
743.571	1995 Jan 26	C	1.49	5 × 10	6.2	3800–7100	2400	

[a] Codes for the data origin are as follows. E: 1.5 m ESO spectroscopic telescope + Boller & Chivens Spectrograph + CCD. E2: 3.6 m ESO telescope + EFOSC1 Spectrograph + CCD. L: 1.6 m LNA telescope + Cassegrain Spectrograph + CCD. C: 2.15 m CASLEO telescope + Cassegrain Spectrograph + CCD. C2: 2.15 m CASLEO telescope + REOSC Spectrograph + CCD.

[b] NOTES.—(1) Photometric. (2) High grating angle. (3) Clouds. (4) Poor seeing, 3″–4″. (5) Focus problem. (6) High humidity. (7) Haze.

conditions of the night. To avoid very long exposures, on most nights three consecutive spectra were obtained; in such cases, the exposure time in Table 1 refers to the sum of the exposures for the individual frames for each night. Note that all spectra cover at least the Hβ–[O III] $\lambda\lambda$4959, 5007 spectral region.

Although the 1.5 m ESO telescope data set is not truly uniform owing to the different gratings used on the different nights, it is at least "nearly uniform" in the sense that the slit was kept at a fixed position angle and with a fixed width, and a constant value for the extraction window was used throughout the data reduction.

Additional spectra were obtained at other observatories. Observations at six epochs were collected at the Complejo Astronomico Leoncito (CASLEO) in Argentina using the 2.15 m telescope with either the Cassegrain or REOSC spectrographs with a CCD detector. Eight more spectra were obtained at the Laboratório Nacional de Astrofisica, Observatório do Pico dos Dias (Brazil) with a Boller & Chivens Spectrograph and a CCD camera on the 1.6 m telescope. Two additional observations were obtained at ESO with the 3.6 m telescope and the EFOSC1.

The spectra from the four different telescopes constitute a large, but quite inhomogeneous, data base. The only subset that is "nearly uniform," as explained above, is the 1.5 m ESO telescope data set. For the rest, even spectra obtained

on a single telescope may differ in aperture geometry and orientation, in addition to the differences in resolution and wavelength range. We therefore must develop systematic corrections that place the observations on a common scale. We emphasize at this point that the signal-to-noise ratio of the light curves we produce is in the end limited by our ability to correct fully for the inhomogeneity of the spectroscopic data. To obtain more accurate spectrophotometric light curves than those presented here requires obtaining homogeneous data from single sources; data obtained with a given instrument should always be obtained *at the very least* with a constant, preferably large, slit width and fixed position angle. Failure to do this compromises the integrity of the data base and can render the data virtually useless.

All spectra were reduced using standard techniques available in either the MIDAS or IRAF software packages. The CCD frames were bias subtracted, and flat-field corrections were applied. Wavelength calibrations are based on comparison lamp spectra taken before and/or after the object exposures. For the ESO 1.5 m telescope data set, the sky background is measured in two regions, on each side of the spectrum, and then an extraction algorithm is applied to obtain a sky-subtracted, one-dimensional spectrum from each frame. Only 11 pixels have been extracted in the spatial direction (i.e., perpendicular to the dispersion), which gives a *constant* 9″ effective slit height. The data are corrected for atmospheric extinction by using a mean extinction curve appropriate for La Silla. The flux calibration is based on standard stars, either LTT 9239 or LTT 377, but both on most occasions, which allowed computation and comparison of two separate response curves that could be used as a quality check. For most nights, the agreement between the two standards is quite good, with the only exceptions of the response curves for two nights (July 14 and Aug 27) when the observation conditions were very poor, as noted in Table 1. On the two worst nights (June 20 and September 24), only one standard was observed, but the nonphotometric conditions are obvious when comparing the three Fairall 9 spectra obtained each night. Finally, all the consecutive Fairall 9 frames taken on one night were averaged together. Similar if not identical procedures were employed in reduction of all of the other spectroscopic data.

Unless otherwise stated, all wavelengths quoted in this paper are in the observed frame and fluxes are observed fluxes not corrected for redshift or interstellar reddening along the line of sight.

2.2. *Absolute Calibration of the Spectra*

As is well known, standard spectrophotometric flux calibration as described in the previous section is generally accurate only to the 10%–15% level, primarily because of (*a*) seeing-dependent light losses at the spectrograph entrance aperture and (*b*) changes in atmospheric transparency. An effective way to attain higher *relative* photometric accuracy in AGN monitoring is to use a method of "internal calibration" based on the assumption that the flux of the narrow emission lines in AGN spectra is constant over the timescales of interest. There are various detailed procedures for achieving this intercalibration of the spectra, some of which are discussed by Baribaud & Alloin (1990). In general, relative photometric accuracy of 1%–2% has been claimed.

The procedure that we use here is to scale all of the spectra in flux by a single multiplicative constant to give a constant measured flux in the narrow [O III] $\lambda\lambda$4959, 5007 emission lines. We have checked the results of our scaling method against those obtained with the automatic scaling procedure of van Groningen & Wanders (1992), and we find close consistency.

The measurement of the [O III] $\lambda\lambda$4959, 5007 line strengths in Seyfert 1 galaxies is not straightforward. In the particular case of Fairall 9, the major sources of difficulty are (*a*) the large width of the Hβ line and (*b*) the strength of the Fe II emission, since a significant contribution from multiplet 42 underlines the Hβ–[O III] region (Fig. 1) of the spectrum. The nuclear spectrum of F9 shows a weak but very broad wing underneath the red side of the [O III] λ5007 line that might be attributed to (*a*) emission from a very broad Hβ red wing, (*b*) Fe II emission, (*c*) a broad [O III] λ5007 component, (*d*) some combination of the above, or (*e*) some unidentified feature. We can reasonably exclude the possibility of very broad Hβ as no similar feature is seen redward of either Hα of Hγ. Fe II emission must contribute to this broad wing, given the observed strength of other Fe II features (Fig. 1), but it does not exclude partial contribution from other sources as well. Further discussion of this feature is beyond the scope of this paper, but we note its presence since it has an effect on our measurement procedures. In order to keep the measurement procedure simple, we have chosen to measure only the narrow [O III] flux, avoiding the flux in the wing underlying it. Therefore, we define a *local* continuum for the [O III] lines as a straight line fitted to the 5150–5161 Å and 5270–5302 Å intervals, and we have summed the intensities of

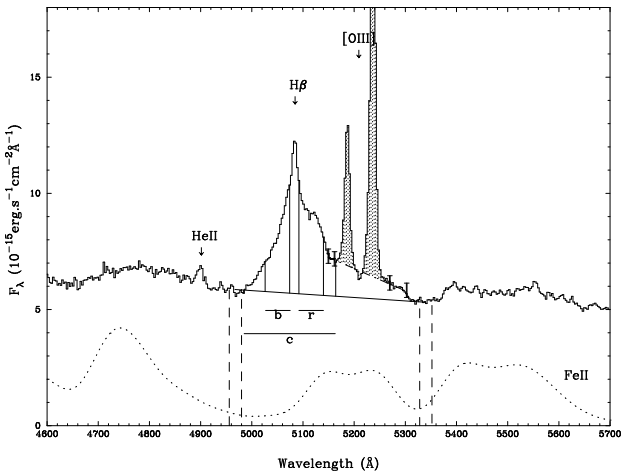

FIG. 1.—Hβ region of the Fairall 9 (F9) spectrum as observed on 1994 May 15 (JD 2,449,487.9). The principal emission lines are identified. The dotted line represents the Fe II emission for a low state of nuclear activity as modeled by Recondo-González et al. (1997). It is shown for comparison only as we have not attempted to deconvolve it from the rest of the emission lines. The method used to measure the continuum and the Hβ and [O III] fluxes is also illustrated. The dot-dashed line delineates the *local*-[O III] continuum approximated by a linear fit in the two regions limited by the small vertical bars. The total [O III] emission is the flux integrated above this line and is represented as the shaded area. The long-dashed vertical lines indicate the two windows where the local-Hβ continuum has been measured, and the straight line interpolated between them is also shown as a thin continuous line. The horizontal lines below Hβ and the thin vertical lines show the spectral ranges where the central (c), blue (b), and red (r) Hβ fluxes have been integrated above the local pseudocontinuum.

both emission lines above this continuum (Fig. 1). To test the efficacy of this procedure, we have also measured the individual [O III] λ5007/[O III] λ4959 flux ratios using this same underlying continuum, and in all cases, the obtained values are close to the theoretical value of 3. However, the mean value (3.17 ± 0.14) is somewhat larger than expected, which indicates that there may be a systematic error in the procedure, the most probable being an underestimation of the [O III] λ4959 flux or, equivalently, an overestimation of the local continuum below it as a result of blending with the broad Hβ wing. This comparison of the fluxes of the two [O III] lines indicates that [O III] λ4959 is about 10% smaller than expected and, therefore, that the total [O III] $\lambda\lambda$4959, 5007 flux loss is only about 3%.

The absolute [O III] λ5007 flux to which all the spectra have been scaled is based on the [O III] λ5007 fluxes measured on the seven photometric nights noted in Table 1, i.e., $F([\text{O III}]\ \lambda5007) = (2.34 \pm 0.03) \times 10^{-13}$ ergs s^{-1} cm^{-2}. All spectra are scaled by a multiplicative constant to match this value. The values of these scale factors are an indication of the level of accuracy one can obtain with standard photometric calibration (i.e., referencing count rates to those measured for standard stars). The mean value of the obtained scaling factors is 1.001 with a rms deviation of 0.257. Most (25 of 29) of the scaling factors are between 0.8 and 1.2. The remaining four are 0.35 and 0.32 for the spectra of June 16 and September 24, respectively, which were obtained under very poor observing conditions (Table 1), and 1.8 and 1.3 for the July 22 and August 31 spectra, respectively.

As mentioned above, we have also used the algorithm of van Groningen & Wanders (1992) to determine the scale factors. This algorithm effects the flux correction by adjusting three free parameters to minimize the residuals in selected narrow emission lines in a difference spectrum formed by subtracting a high-quality reference spectrum from each of the observations. The adjustable parameters are the flux scaling factor, a relative linear wavelength shift between the two spectra, and a relative convolution factor that accounts for small resolution differences between the two spectra. By varying these initial parameters, the program finds the optimal solution that minimizes the residuals of the fit.

The comparison of the scaling factors yielded by both methods shows that they are consistent within 4%, and the mean values agree to $1.4\% \pm 1.1\%$ if we consider only the ESO 1.5 m data set. If we consider all the spectra, the differences are always smaller than 10%, and the mean values of the scaling factors agree to $4\% \pm 5\%$. We adopt these as measures of the internal accuracy of the fluxes and therefore assume that the accuracy of the internal calibration of the ESO 1.5 m data set is $\sim$1.4% and that of the entire data set $\sim$5%. However, for those few ESO spectra for which the scaling factors greatly differ from unity (as described above), we will assign uncertainties of 3%. These uncertainty estimates do not take into account possible systematic errors.

The absolute flux we adopt, $F([\text{O III}]\ \lambda5007) = (2.34 \pm 0.03) \times 10^{-13}$ ergs s^{-1} cm^{-2}, is in good agreement with previously published measurements. These include $F([\text{O III}]\ \lambda5007) = (2.33 \pm 0.12) \times 10^{-13}$ ergs s^{-1} cm^{-2} (Lub & de Ruiter 1992), $F([\text{O III}]\ \lambda5007) = 2.40 \times 10^{-13}$ ergs s^{-1} cm^{-2} (Whittle 1985), and $F([\text{O III}]\ \lambda5007) = (2.18 \pm 0.65) \times 10^{-13}$ ergs s^{-1} cm^{-2} (Stirpe, van Groningen, & de Bruyn 1989). Comparison of these values with our measurement is not straightforward as it is not specified in the literature how the [O III] λ5007 flux is measured and whether the reported values include the flux in the "[O III]–wing" or the Fe II λ5018 emission. Neither of these appear to contribute significantly to our measurements, although a small contribution from Fe II cannot be excluded. We estimate that the systematic uncertainty of our absolute fluxes is of order 10%.

3. THE NUCLEAR CONTINUUM EMISSION

3.1. *Measurement of the Nuclear Continuum*

The optical continuum flux measured from the spectra consists of at least two components: (1) the variable AGN component (referred to hereafter as the "nuclear component," which arises in a pointlike source, and (2) a spatially extended but presumably constant component, which results from the integrated light of stars in the host galaxy. Separation of these two components is not straightforward and is complicated by how the observed surface brightness distributions of these two components change with atmospheric seeing; the ratio of nuclear light and host-galaxy light recorded through a fixed aperture geometry varies with seeing. In principle, it is possible to correct for these aperture effects if the seeing is measured and one has a good model for the host-galaxy surface brightness distribution (see, e.g., Wanders et al. 1992); even if a formal correction cannot be made, aperture effects can be reduced by using a fixed aperture geometry with dimensions larger than the worst seeing one expects to encounter (Peterson et al. 1995). In practice, it is possible to determine empirically adjustments for aperture effects between contemporaneous light curves, as has been done in other International AGN Watch programs (see, e.g., Peterson et al. 1994, and references therein), provided that the individual data sets are internally homogeneous. Unfortunately, in this experiment, only the ESO 1.5 m telescope data (set E) were obtained through a fixed entrance aperture, and therefore only this data set can be used to measure the optical continuum.

The continuum flux has been measured in the only nominally emission-line–free window covered in all the spectra, that is, between the strong [O III] λ5007 line and the Fe II blend longward of this feature. In the observed frame, this continuum window lies at an observed central wavelength of 5340 Å and a width of 24 Å (Fig. 1). Another spectral window that is relatively free of emission lines is immediately shortward of Hβ, centered at 4967 Å and 24 Å wide. However, it is potentially contaminated by both the very broad wings of Hβ and He II λ4686, and therefore, it will be used only to estimate a local pseudocontinuum under the Hβ–[O III] region that will be used for the purpose of Hβ emission-line measurements, as described below. Table 2 gives the measured values of the 5340 Å average flux density, and Figure 2 plots them as a function of time. The quoted errors are the quadratic sum of the 1.4% (or 3% for a few cases; see above) uncertainty in the internal calibration plus the rms deviation around the mean flux in the continuum window. The largest of these contributions is always the internal calibration uncertainty.

Fairall 9 is sufficiently distant from Earth that the angular size of the host galaxy is quite small (0.″8 × 0.″7), which means that even small apertures include a large fraction of the total light from the galaxy. The problem is not critical because of the weakness of the galaxy relative to the active nucleus, but the contribution from the galaxy is nonetheless nonnegligible. At an observed wavelength of

TABLE 2

OPTICAL CONTINUUM LIGHT CURVE

Julian Date (−2,449,000) (1)	F_λ(5340 Å) (10^{-15} ergs s^{-1} cm^{-2} Å^{-1}) (2)
475.924.....	5.56 ± 0.09
479.930.....	5.56 ± 0.09
483.933.....	5.36 ± 0.08
487.922.....	5.31 ± 0.08
491.924.....	5.55 ± 0.08
499.909.....	5.52 ± 0.09
511.930.....	5.72 ± 0.08
515.904.....	5.51 ± 0.08
519.932.....	5.73 ± 0.16
523.929.....	5.86 ± 0.08
531.918.....	5.78 ± 0.08
535.919.....	5.65 ± 0.08
539.883.....	5.44 ± 0.08
543.900.....	5.66 ± 0.08
547.908.....	5.37 ± 0.08
555.910.....	6.05 ± 0.17
559.905.....	5.32 ± 0.08
567.884.....	5.60 ± 0.08
575.861.....	5.83 ± 0.08
579.852.....	5.99 ± 0.08
591.809.....	5.94 ± 0.08
595.776.....	6.44 ± 0.18
599.736.....	5.92 ± 0.09
607.731.....	6.83 ± 0.10
619.733.....	6.36 ± 0.19
623.725.....	6.36 ± 0.09
626.676.....	6.59 ± 0.09
653.739.....	7.88 ± 0.13
664.676.....	7.86 ± 0.11

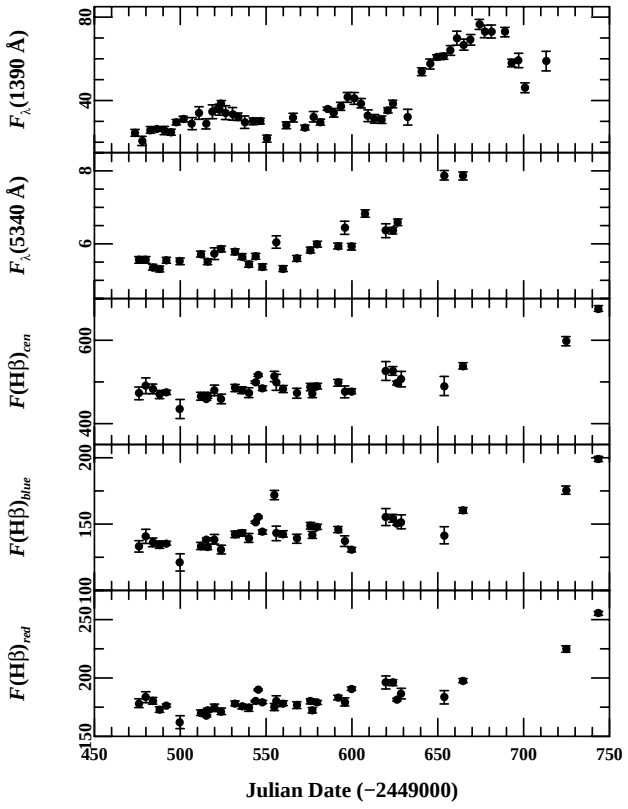

FIG. 2.—From top to bottom, we show first the 1390 Å UV continuum light curve (from Paper IX), next the 5340 Å optical continuum light curve (Table 2), and then the $H\beta_{cen}$, $H\beta_{blue}$, and $H\beta_{red}$ fluxes (Table 4). The errors associated with the optical points do *not* include the uncertainty in the absolute calibration, as described in the text.

5340 Å, a direct comparison of the fluxes in two pairs of spectra that are nearly simultaneous in time and are taken with different apertures suggests that the stellar contribution for an aperture of 6″ × 10″ is $\sim 1 \times 10^{-15}$ ergs s^{-1} cm^{-2} Å^{-1} larger than that within a 4″ × 9″ rectangular aperture. The total flux through the smaller of these apertures is about 5.5×10^{-15} ergs s^{-1} cm^{-2} Å^{-1}.

The host-galaxy contribution through a given aperture geometry can be estimated by integrating a model of the galaxy surface brightness distribution. Since we were unable to obtain a good photometric image of F9 under good seeing conditions, for this analysis we used published azimuthally averaged radial surface brightness distributions, as discussed recently by Recondo-González et al. (1997), from Griersmith & Visvanathan (1979), Lub & de Ruiter (1992), and Véron-Cetty, Woltjer, & Roy (1991). The consistency of the results by these three groups is discussed by Recondo-González et al. (1997), who find a good agreement between Griersmith & Visvanathan and Véron-Cetty et al., while the galactic fluxes in F9 derived by Lub & de Ruiter are smaller by a factor ∼2, probably because the exponential disk profile they consider is less suitable than the $r^{1/4}$ bulge law used by Griersmith & Visvanathan and Véron-Cetty et al. Using the Griersmith & Visvanathan decomposition, we obtain a galaxy flux of 2.7×10^{-15} ergs s^{-1} cm^{-2} Å^{-1} and 3.3×10^{-15} ergs s^{-1} cm^{-2} Å^{-1} through circular apertures of $r = 3''.39$ and $r = 4''.37$, respectively (equivalent to 4″ × 9″ and 6″ × 10″, in the sense that they cover equal areas). This means $\sim 0.6 \times 10^{-15}$ ergs s^{-1} cm^{-2} Å^{-1} more flux in the larger of the two apertures, consistent with the estimate obtained by subtracting contemporaneous spectra, as described above.

4. THE Hβ EMISSION LINE

The flux of Hβ was measured by fitting a linear continuum between the intervals 4956–4980 Å and 5328–5352 Å and integrating the flux above the estimated continuum between 4985 and 5163 Å, similar to what has been done in the case of NGC 5548 (Peterson et al. 1991) and NGC 3783 (Stirpe et al. 1994). The integration range is shown as "c" in Figure 1. We refer to this measurement hereafter as the "central Hβ flux" $F(H\beta)_{cen}$. $F(H\beta)_{cen}$ includes the flux between radial velocity $v_r = -5900$ km s^{-1} to $v_r = 4600$ km s^{-1}, where v_r is measured relative to the peak of the Hβ narrow component. Larger radial velocities were excluded to avoid possible contamination by other species. This measurement includes only part of the broad Hβ component and does not include the flux in the very broad Hβ red wing, which as noted above, we believe is primarily contaminating emission. The Hβ narrow component emission is also included in $F(H\beta)_{cen}$, but its contribution should be constant, and at worst it will only decrease the contrast of the light curves. The fluxes in the blue and red wings of Hβ [included in $F(H\beta)_{cen}$] have also been measured separately. They are computed as the total flux above the continuum between radial velocity $v_r = 400$ km s^{-1} and $v_r = 3200$ km s^{-1}, hereafter called $F(H\beta)_{red}$ and shown as "r" in Figure 1, and $v_r = -400$ km s^{-1} and $v_r = -3200$ km s^{-1}, hereafter called $F(H\beta)_{blue}$ and shown as "b" in Figure 1. As for $F(H\beta)_{cen}$, larger radial velocities have been avoided because of possible blendings with other features.

As noted above, the various data sets often show systematic offsets relative to one another, and these are generally attributed to aperture effects. In the case of these data, we

have compared measurements of $F(\mathrm{H}\beta)_{\mathrm{cen}}$ from the different data sets based on closely spaced observations. We find that observations separated by less than 2 days can be brought into close agreement by multiplicatively scaling the measurements from sets C and L by a constant. The constants required to bring the light curves from sets E, L, and C into agreement are given in Table 3.

Table 4 lists and Figure 2 plots the values of $F(\mathrm{H}\beta)_{\mathrm{cen}}$, $F(\mathrm{H}\beta)_{\mathrm{blue}}$, and $F(\mathrm{H}\beta)_{\mathrm{red}}$, all suitably adjusted to a common scale by multiplying the measured values by the scaling constants given in Table 3. The error bars displayed include the propagation of the uncertainties in the continuum under each line (measured as the rms deviation of the mean in each of the two continuum windows in which it is computed). Other possible uncertainty sources should give rise to smaller errors. For instance, the corrections applied to account for systematic offsets between different data sets or the differences on aperture within the sets may have left some residual scaling errors on individual points, but they are not considered.

TABLE 3

SCALING PARAMETERS

Data Set (1)	Scaling Factor (2)
E	1.000
L	1.123 ± 0.046
C	1.071 ± 0.048

TABLE 4

Hβ LIGHT CURVES

Julian Date ($-2{,}449{,}000$) (1)	$F(\mathrm{H}\beta)_{\mathrm{cen}}$ [a] (2)	$F(\mathrm{H}\beta)_{\mathrm{blue}}$ [a] (3)	$F(\mathrm{H}\beta)_{\mathrm{red}}$ [a] (4)
475.925.....	472.6 ± 15.2	133.2 ± 4.3	178.4 ± 3.8
479.930.....	490.8 ± 18.9	140.8 ± 5.3	183.5 ± 4.7
483.933.....	483.3 ± 11.6	136.2 ± 3.3	180.5 ± 2.9
487.923.....	469.8 ± 9.7	134.5 ± 2.8	173.0 ± 2.4
491.931.....	475.1 ± 5.2	135.6 ± 1.5	176.4 ± 1.3
499.909.....	435.1 ± 22.8	121.1 ± 6.5	162.2 ± 5.5
511.930.....	465.7 ± 9.5	133.5 ± 2.7	170.2 ± 2.3
515.339.....	459.5 ± 3.5	138.6 ± 1.0	167.5 ± 0.9
515.904.....	467.5 ± 7.1	132.8 ± 2.0	172.4 ± 1.8
519.932.....	479.7 ± 12.8	138.6 ± 3.6	174.5 ± 3.2
523.929.....	459.2 ± 11.5	130.8 ± 3.3	171.4 ± 2.8
531.918.....	485.4 ± 8.7	142.3 ± 2.5	178.2 ± 2.1
535.919.....	480.3 ± 8.1	143.2 ± 2.3	175.5 ± 2.0
539.884.....	474.3 ± 11.8	139.6 ± 3.3	174.4 ± 2.9
543.630.....	499.4 ± 2.9	151.4 ± 0.8	180.2 ± 0.7
545.359.....	516.3 ± 3.0	155.2 ± 0.9	189.9 ± 0.7
547.916.....	484.8 ± 5.5	144.0 ± 1.5	179.4 ± 1.4
554.826.....	513.1 ± 12.3	171.9 ± 3.5	175.1 ± 3.0
555.910.....	499.1 ± 19.2	143.0 ± 5.5	180.1 ± 4.6
559.905.....	483.1 ± 8.4	142.6 ± 2.4	178.4 ± 2.1
567.884.....	472.9 ± 11.9	138.9 ± 3.4	176.7 ± 2.9
575.861.....	487.7 ± 8.9	148.8 ± 2.5	180.0 ± 2.2
576.925.....	471.6 ± 9.2	141.9 ± 2.6	172.3 ± 2.3
579.852.....	489.9 ± 6.9	147.9 ± 1.9	179.0 ± 1.7
591.809.....	497.9 ± 8.1	145.9 ± 2.3	183.2 ± 2.0
595.777.....	476.2 ± 14.2	137.2 ± 4.0	179.5 ± 3.5
599.738.....	477.7 ± 6.1	130.7 ± 1.7	190.8 ± 1.5
619.733.....	526.3 ± 22.6	155.3 ± 6.4	196.2 ± 5.6
623.725.....	526.5 ± 10.4	154.4 ± 2.9	196.0 ± 2.6
626.185.....	497.3 ± 4.6	150.5 ± 1.3	181.4 ± 1.1
628.733.....	506.8 ± 18.6	151.7 ± 5.2	186.6 ± 4.6
653.740.....	490.3 ± 22.9	141.6 ± 6.4	183.5 ± 5.7
664.676.....	538.6 ± 7.5	160.3 ± 2.1	197.7 ± 1.8
724.604.....	597.7 ± 11.0	175.6 ± 3.1	224.8 ± 2.7
743.571.....	676.1 ± 6.9	199.1 ± 1.9	255.4 ± 1.7

[a] Units are 10^{-15} ergs s^{-1} cm^{-2} Å^{-1}.

5. THE PATTERN OF VARIABILITY

5.1. *Amplitudes and Timescales*

The light curves in Figure 2 clearly show the variations of the optical flux at 5340 Å and the lower amplitude variability of the Hβ fluxes. Table 5 summarizes some simple characteristics of the continuum and Hβ variability. Column (1) lists the individual spectral features. Column (2) gives the unweighted mean and rms flux averaged over all observations, and column (3) gives the fractional variation F_{var} (defined as the ratio of the rms to the mean flux, after subtraction of the measurement error in quadrature; see Paper IX). The ratio of maximum flux to minimum flux R_{max} appears in column (4).

The mean optical continuum level from Table 5 is $F_\lambda(5340\ \text{Å}) = 5.95 \times 10^{-15}$ ergs s^{-1} cm^{-2} Å^{-1}. Following the discussion above, we subtract an estimated value of $F_\lambda(5340\ \text{Å})_{\mathrm{gal}} = 2.7 \times 10^{-15}$ ergs s^{-1} cm^{-2} Å^{-1} to account for the starlight from the underlying galaxy through the $4'' \times 9''$ aperture, which yields a mean *nuclear* flux of $F_\lambda(5340\ \text{Å})_{\mathrm{nuc}} = 3.3 \times 10^{-15}$ ergs s^{-1} cm^{-2} Å^{-1}, as given in Table 5. This value is close to the recorded historical minimum for F9, as is also found for the UV continuum during the same epoch (Paper IX). Further comparisons can be made with optical fluxes reported by Lub & de Ruiter (1992) and with the historical V light curve from Recondo-González et al. (1997). The latter has been inferred from the measurements of the optical photomultiplier (the FES) on board the *IUE* satellite. After adjusting the published values to observed, uncorrected fluxes and adjusting to common starlight corrections, we can safely conclude that the continuum level of the active nucleus in F9 was close to or at its historical minimum during most of the monitoring campaign of 1994.

The maximum amplitude variations (R_{max}) of the 5340 Å flux are significantly smaller than those of the fluxes in the different UV bands (ranging from $R_{\mathrm{max}} = 3.72 \pm 0.42$ at 1390 Å to $R_{\mathrm{max}} = 2.68 \pm 0.24$ at 1880 Å). This confirms the general trend reported in Paper IX that the amplitude of the variations decreases at longer wavelengths. In Paper IX, it was argued that, in contrast to the general wisdom that AGN UV/optical spectra vary with larger amplitude at shorter wavelengths, the amplitude of continuum variation in F9 appears to be independent of wavelength and that the apparently decreasing amplitude of variability with increasing wavelength is simply the result of increasing contami-

TABLE 5

VARIABILITY PARAMETERS

Feature (1)	Mean and RMS Flux[a] (2)	F_{var} (3)	R_{max} [b] (4)
F_λ(5340 Å).....	5.95 ± 0.66	0.110	1.48 ± 0.03
F_λ(5340 Å)$_{\mathrm{nuc}}$.....	3.25 ± 0.66	0.200	1.98 ± 0.08
Hβ_{cen}.....	495 ± 42	0.082	1.55 ± 0.08
Hβ_{blue}.....	145 ± 14	0.097	1.64 ± 0.09
Hβ_{red}.....	183 ± 17	0.090	1.57 ± 0.06

[a] Units are 10^{-15} ergs s^{-1} cm^{-2} Å^{-1} for the continuum and 10^{-15} ergs s^{-1} cm^{-2} for Hβ.

[b] Ratio between maximum and minimum values. Uncertainties calculated by propagation of 1 σ flux errors.

nation by a constant component. Following the arguments in Paper IX, Figure 3 plots the optical continuum fluxes versus the contemporaneous (i.e., within 2 days) ultraviolet fluxes (however, we have excluded the optical point measured on JD 2,449,607, which we regard as suspiciously high). If the amplitude of variation of the nuclear continuum is independent of wavelength, these data should show a linear relationship, and the intersection of the best-fit line with the optical axis should give an estimate of the constant-component flux (principally starlight) at 5340 Å. The best-fit line to these data gives a constant-component flux of $F_\lambda(5340\ \text{Å}) = 3.89 \times 10^{-15}$ ergs s^{-1} cm^{-2} Å^{-1}, i.e., 44% *larger* than the starlight flux estimated by integration of the galactic surface brightness distribution. If we subtract the constant-component flux from the measured optical fluxes, we find that a power-law fit of the form

$$\log F_\lambda(5340\ \text{Å})_{\text{nuc}} \propto \gamma \log F_\lambda(1390\ \text{Å}) \qquad (1)$$

yields a slope $\gamma = 1.002 \pm 0.081$, i.e., a linear relationship. The difference between the estimated galaxy flux $F_\lambda(5340\ \text{Å})_{\text{gal}} = 2.7 \times 10^{-15}$ ergs s^{-1} cm^{-2} Å^{-1} and the constant-component flux $F_\lambda(5340\ \text{Å}) = 3.9 \times 10^{-15}$ ergs s^{-1} cm^{-2} Å^{-1} inferred from Figure 3 is plausibly attributable to additional contamination of the 5340 Å continuum by Fe II emission. The amount of Fe II emission estimated by Recondo-González et al. (1997) for a low state of activity of F9, as shown in Figure 1, apparently accounts for the difference in these values. This suggests that, at least during the 1994 campaign, the decrease in the amplitude of the 5340 Å flux variations relative to the 1390 Å variations can be accounted for by dilution of the optical continuum by a combination of stellar light and Fe II emission only, rather than by "hardening" of the continuum as it brightens. This result is in agreement with that of Recondo-González et al. (1997), who find that the UV and optical fluxes vary in strict proportion even during the large amplitude of variations recorded from 1978 to 1991. Another example of an AGN that maintains a constant UV/optical spectral energy distribution while its intensity changes is the low-luminosity Seyfert 1 galaxy NGC 4593 (Santos-Lleó et al. 1995). This is contrary to what has been concluded in other cases.

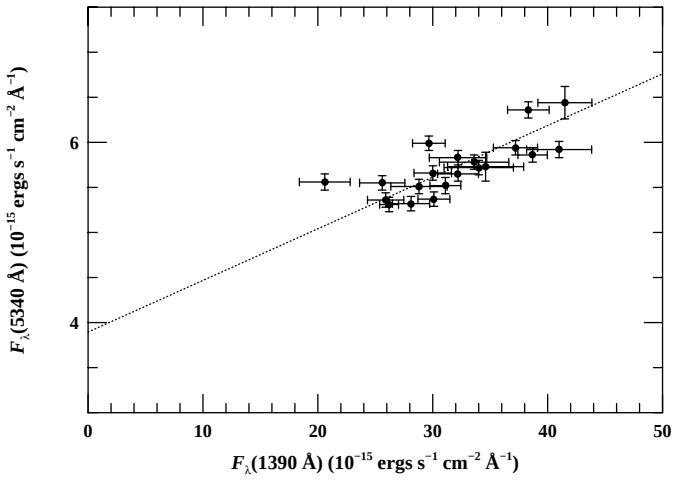

FIG. 3.—Measured $F_\lambda(5340\ \text{Å})$ continuum fluxes are plotted on a linear scale against contemporaneous (i.e., within 2 days) UV fluxes $F_\lambda(1390\ \text{Å})$ from Paper IX. The dotted line shows the best-fit linear relationship between these parameters, which intersects the y-axis at $F_\lambda(5340\ \text{Å}) \approx 3.9 \times 10^{-15}$ ergs s^{-1} cm^{-2} Å^{-1}.

Comparison of the 1390 and 5340 Å light curves in Figure 2 shows that the variations in the two bands are similar and apparently in phase, despite the absence of optical data during the most significant variations near the end of the campaign; the only indication of this large event in the optical light curve is that the last two data points are well above the mean level of the rest of the previous data. For the first two events, the amplitude of the optical variations ($\sim$10% and 20% for the first and second events, respectively) is smaller than in the UV ($\sim$50%), but the nuclear optical variations are similar to those in the UV.

Close inspection of the point-to-point variations of the continuum flux shows that no significant variations are seen on 4 day timescales, which is the minimum timescale of variability that can be studied with these data. Very slight variations (4%–5%) are seen on six occasions, but only at the 2 σ level. On somewhat longer timescales, fluctuations up to 12% in 20 days and 24% in 30 days (at the 5.7 and 9.5 σ level, respectively) are detected. The largest change detected, with $R_{\text{max}} = 1.48 \pm 0.03$ (Table 5), took place over 94 days.

Table 5 and Figure 2 show that the Hβ variability amplitude is smaller than that of the optical continuum. Part of this effect can be explained by the contribution to the Hβ flux of other sources that are either (*a*) constant or (*b*) variable but on a timescale different from broad-line Hβ. The most important contributions are due to Fe II and narrow Hβ emission (see Fig. 1). Another, less important, contribution is the Hβ absorption from the underlying starlight. We estimate that it is less than 2% of the average $\text{H}\beta_{\text{cen}}$ intensity, using the strength of the stellar continuum and the typical equivalent widths of Hβ absorption in the bulge of early-type spirals (e.g., from 3.4 to 3.9; Bica 1988). These contaminating contributions are less important for $\text{H}\beta_{\text{red}}$ and almost negligible for $\text{H}\beta_{\text{blue}}$, and indeed both the $\text{H}\beta_{\text{red}}$ and $\text{H}\beta_{\text{blue}}$ components exhibit larger values of F_{var} than the central Hβ fluxes. However, the variability parameters of the $\text{H}\beta_{\text{blue}}$ flux still indicate that the intrinsic Hβ amplitude of variability is still smaller than that of the continuum flux, as has been found in other well-monitored AGNs.

5.2. *Cross-Correlation Analysis*

In order to quantify the relationship between the various light curves presented here and in Paper IX, we have carried out a simple cross-correlation analysis. Cross-correlation functions (CCFs) have been computed by using two different algorithms: the interpolation method of Gaskell & Sparke (1986) and the discrete correlation function (DCF) of Edelson & Krolik (1988). In each case, the specific algorithms used are as described by White & Peterson (1994). Both methods give the same results, as is generally the case for reasonably well-sampled data. Figure 4 plots the CCFs. The top panel shows both the UV/optical continuum CCF as well as the UV continuum autocorrelation function (ACF) for comparison. The next three panels show the results of cross-correlating the $\text{H}\beta_{\text{cen}}$, $\text{H}\beta_{\text{blue}}$, and $\text{H}\beta_{\text{red}}$ light curves with the 1390 Å continuum light curve, and the bottom panel shows direct cross-correlation of $\text{H}\beta_{\text{blue}}$ and $\text{H}\beta_{\text{red}}$. Table 6 summarizes the important features of the CCFs. Columns (1) and (2) give the two time series that are cross-correlated. Column (3) gives the location of the peak in the CCF that is nearest to zero lag, since the other peaks are almost certainly aliases; positive lags are in the sense that the second series is delayed relative to the first. Column

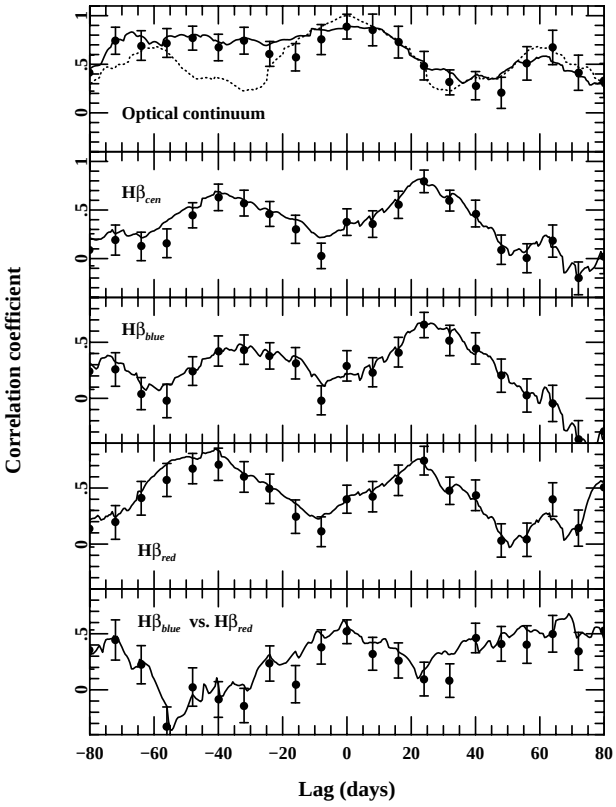

FIG. 4.—Cross-correlation functions (CCFs), based on the light curves shown in Fig. 2. The upper panel shows as a solid line the result of cross-correlating the 1390 Å UV continuum light curve with the 5340 Å optical continuum light curve. The filled circles with error bars show the discrete correlation function (DCF) values. The dotted line shows the UV continuum autocorrelation function for the subset of the light curve (JD 2,449,473.6 to JD 2,449,657.4) used in the calculations here. The middle three panels show the results of correlating the 1390 Å light curves with those for $H\beta_{cen}$, $H\beta_{blue}$, and $H\beta_{red}$, respectively, as given in Table 4. The bottom panel shows the direct cross-correlation of $H\beta_{blue}$ and $H\beta_{red}$.

(4) gives the centroid of this peak τ_{cent}, and its maximum value r_{max} is given in column (5). The value of τ_{cent} is computed using all points in the peak above $0.8r_{max}$. Column (6) gives the full width at half-maximum (FWHM) for each CCF. The CCFs shown in Figure 4 and summarized in Table 6 were computed using only the parts of the light curves that strongly overlap; specifically, UV and optical data after JD 2,449,665 were not used in the calculations.

TABLE 6

CROSS-CORRELATION RESULTS

First Series (1)	Second Series (2)	τ_{peak} (days) (3)	τ_{cent} (days) (4)	r_{max} (5)	FWHM (days) (6)
F_λ(1390 Å)	F_λ(1390 Å) (ACF)	0.	0.	1.00	47
F_λ(5340 Å)	F_λ(5340 Å) (ACF)	0.	0.	1.00	170
F_λ(5340 Å)[a]	F_λ(5340 Å)[a] (ACF)	0.	0.	1.00	47
F_λ(1390 Å)	F_λ(5340 Å)	1	−3.6	0.89	109
F_λ(1390 Å)	F_λ(5340 Å)[a]	0	−2.4	0.70	39
F_λ(1390 Å)	$F(H\beta)_{cen}$	23	23.0	0.82	33
F_λ(1390 Å)	$F(H\beta)_{blue}$	23	26.7	0.67	33
F_λ(1390 Å)	$F(H\beta)_{red}$	23	21.8	0.76	42
$F(H\beta)_{blue}$	$F(H\beta)_{red}$	−1	−0.8	0.62	32

[a] Subset from JD 2,449,475.9 to JD 2,449,626.7, excluding JD 2,449,555.9 and JD 2,449,607.7.

The peak of the UV/optical continuum cross-correlation is near a value of zero lag, but it is fairly broad and rather poorly defined. The strongest variations in the optical continuum occur at the very end of the campaign, when the light curves are poorly sampled. The results should thus be quite sensitive to the 27 day gap that occurred immediately before the two final observations. Furthermore, there are two points in the optical continuum light curve that we regard as suspiciously high, at JD 2,449,555 and JD 2,449,607. We have therefore defined a "best subset" of the optical continuum data, which extends from the beginning of the campaign and ends with the observation on JD 2,449,626 and excludes the two suspicious points. We then cross-correlated this reduced subset of 25 points with the part of the UV light curve that overlaps with them. Figure 5 compares the results for both versions of the optical continuum light curve. Table 6 summarizes the results for both.

Table 6 also summarizes the UV continuum/Hβ CCFs shown in Figure 4. The peaks of the continuum/line CCFs indicate a line flux lag of 23 days. Here the CCFs are based on the light curves up through JD 2,449,664.7; we also computed the CCFs using the data only from the best sampled part of the Hβ light curves, through JD 2,449,628.7, but the results were nearly identical. We also cross-correlated the 1390 Å light curve with only the most homogeneous Hβ measurements, those from the ESO 1.5 m telescope (set E), and again the results did not change. We thus regard the measured Hβ lag as quite robust.

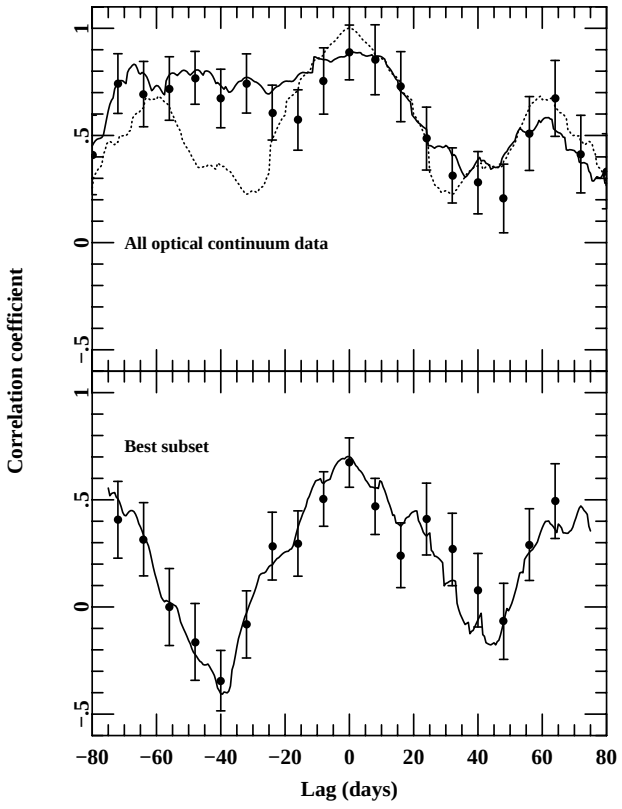

FIG. 5.—The top panel shows the CCF computed by cross-correlating the entire optical continuum light curve (as in Table 2 and Fig. 2) with the overlapping part of the 1390 Å UV light curve from Paper IX (also shown in Fig. 2). The lower panel shows the CCF that is obtained by reducing the length of the UV and optical light curves to avoid interpolating across the 27 day gap near the end of the optical light curve, and with two suspiciously high optical continuum points (at JD 2,449,555 and JD 2,449,607) excluded. The filled circles show the corresponding DCF values.

The uncertainties in the cross-correlation results have been estimated by running Monte Carlo simulations as described by White & Peterson (1994). The same procedure was applied to the results of the UV campaign in Paper IX. We find that the uncertainties in the UV/optical continuum lag and in the Hβ lag are about 1–2 days and about 2–3 days, respectively.

Finally, we also cross-correlated the blue wing and red wing Hβ fluxes directly in order to test for gross radial motions within the BLR. Table 6 and the bottom panel of Figure 4 show that there is no lag detected between the blue and red sides, which thus rules out predominantly radial motion of the Hβ-emitting gas.

5.3. Hβ *Profile Variations*

Emission-line profile variability is of interest in that it can provide strong constraints on kinematical models of the BLR. A convenient way to search for line profile variations is by comparing the mean and rms spectra computed from a well-sampled time series of spectra, such as we have here. The upper panel in Figure 6 shows the 4600–5900 Å range mean spectrum together with the rms variations about this mean. To compute these spectra, individual absolute intercalibrated spectra have been convolved to a common resolution (that of the ESO spectrum from JD 2,449,531). Spectra of lower resolution were excluded from this computation, as were all spectra we regard as of lower or dubious quality (usually because of poor observing conditions, as noted in Table 1). A total of 18 spectra have been used to compute the mean and rms spectra.

Mean "high"-state and "low"-state spectra have also been computed. The high-state spectrum is the average of the spectra taken on JD 2,449,665, JD 2,449,654, JD 2,449,627, and JD 2,449,624 and the low-state spectrum is the average of the spectra from JD 2,449,476, JD 2,449,480, JD 2,449,484, JD 2,449,488, and JD 2,449,512. All spectra were convolved to the same resolution before averaging. The second panel of Figure 6 shows both spectra and their difference.

Finally, the difference between two individual spectra has also been computed (Fig. 7) based on the single highest state spectrum (JD 2,449,665) and the single lowest state spectrum (JD 2,449,488). Both spectra were obtained with the same telescope and instrument configuration, and no correction for resolution has therefore been applied. The range covered by the difference spectrum is larger than that shown in Figure 6, from $\sim$4500 Å up to $\sim$7880 Å. The amplitude of the variations decreases from $\sim$5200 Å to $\sim$6000 Å. There is an increase of the amplitude of the variations in the wavelength region of He I λ5876. To the red, the variations remain more or less with the same amplitude until the blue wing of Hα is reached.

It is clear from Figures 6 and 7 that small, but significant, line profile variations have occurred in Hβ during the 1994 optical campaign. Figure 7 shows that Hα has experienced similar changes, although an atmospheric absorption feature at $\sim$6865 Å (the telluric O_2 *B* band) does not subtract out cleanly and therefore did not allow a detailed comparison of the red part of the Hβ and Hα profiles. The Hβ line variations (both in the rms and difference spectra) exhibit two clear components, one longward and one short-

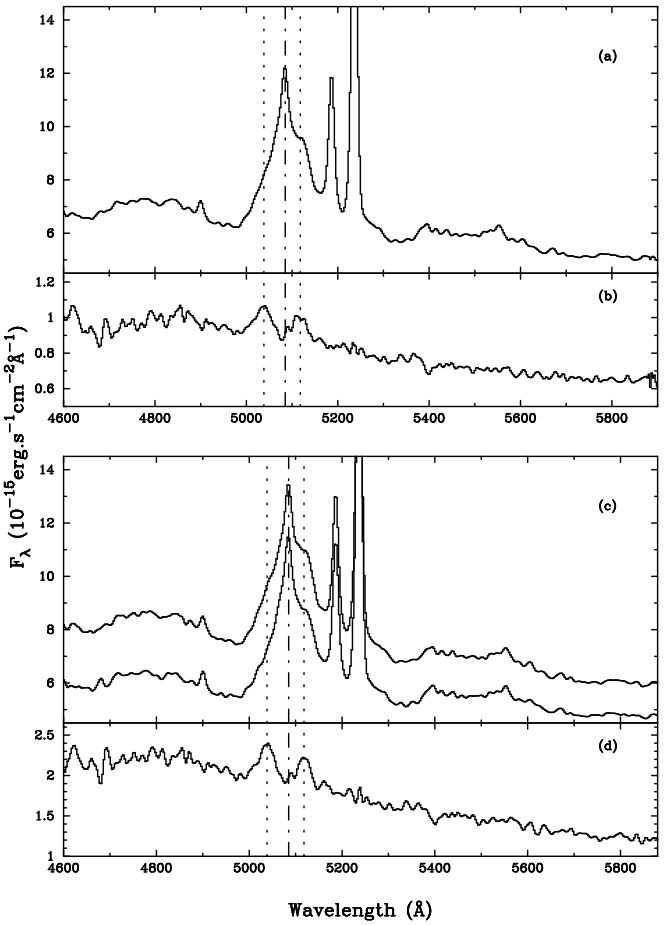

FIG. 6.—(*a*) The average of the best ESO spectra, convolved to the same resolution. (*b*) The rms deviations about the above average. (*c*) The mean "high" state and "low" state spectra. (*d*) Difference between the two spectra shown in (*c*). The narrow Hβ peak is indicated with a dot-dashed line and the peaks of the two Hβ components (see text) as dotted lines.

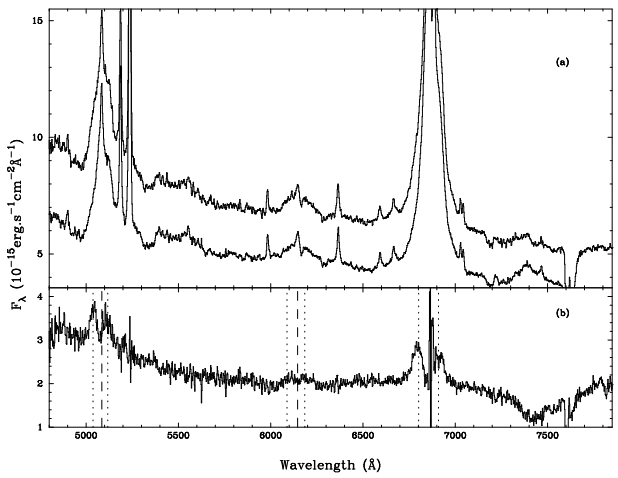

FIG. 7.—(*a*) The spectra obtained at ESO on 1994 November 8 (JD 2,449,664.7) (higher state) and 1994 May 15 (JD 2,449,487.9) (lower state). (*b*) The difference between the spectra in (*a*). Notice that the continuum and the broad lines all increased. In particular, as is also shown in Fig. 6, the hydrogen Balmer-line difference profiles show a clear two-component structure. As in Fig. 6, the dotted lines indicate the peak position of these two components in Hβ or the position where they should be if He I λ5876 and Hα had the same structure. The dashed lines indicate the positions of the narrow-line peaks. The broad dip near 7450 Å in (*b*) is a calibration artifact, due to the differences in the response functions estimated from the standard stars. The residuals near 7600 Å are due to the telluric A band.

ward of the line center. The Hα difference profile shows a similar two-component structure. Comparison of the blue variable components of Hα and Hβ gives and Hα/Hβ ratio of 2.1 ± 0.4. This value is quite low as compared to the ratio usually found in the BLR of Seyfert 1 galaxies (from 4 to 6) but is not significantly different from the recombination case B value of 2.8. The He I λ5876 fluctuations, though very noisy, are also double peaked. In contrast, the variable part of the He II λ4686 line does *not* show any clear indication of a two-component structure. The He II λ4686 fluctuations could be described in terms of a single very broad component that is slightly blueshifted. The Fe II blend at ~5370–5620 Å (observed wavelengths) seems to remain constant during the entire monitoring campaign. Nevertheless, both the He II λ4686 and the Fe II are weak features. Their possible fluctuations (in the rms and difference spectra) are very noisy, and a more careful analysis should be performed.

Double-peaked broad-line profiles or variability profiles have already been reported for a small number (25–30) of AGNs, most of them radio loud (see, e.g., Puchnarewicz, Mason, & Carrera 1996 and references therein). The interpretation of these features is still controversial and beyond the scope of this paper. Merely for the sake of description and not as a physical model, we have fitted the Hβ difference and rms profiles with two Gaussians above a linear continuum. The two best-fit Gaussians are characterized by velocities relative to the narrow Hβ peak of about −2800 and +1900 km s^{-1} and corresponding widths of 2500 and 2200 km s^{-1} (FWHM), respectively. Their intensity ratio is ~1.3, with the blue component the brightest. This scheme resembles the profile decomposition by Recondo-González et al. (1997) for the UV lines in Fairall 9. Apart from two central components (one narrow and another broad), these authors find two additional broad components: one centered at $v_r \approx +3300$ km s^{-1} longward of line center and another one at $v_r \approx -3600$ km s^{-1} shortward of the line center. Both have similar widths, 5800 km s^{-1} and 5900 km s^{-1}, respectively. Although the positions of the UV-line components are clearly compatible with those found for the rms and the difference Hβ profile, their widths are larger.

Not only does the F9 Hβ profile vary, but the profile variations are also variable themselves. During a previous optical monitoring campaign in 1991–1992 (Winge et al. 1996), in the difference between two spectra, taken 4 months apart, the variable Hβ profile is well described by a quite smooth, blueshifted component. Also, Wamsteker et al. (1985) find that the difference Hβ profile between two spectra obtained on 1981 December and 1982 November, shows an enhanced red shoulder, which they characterize by a Gaussian component 1650 km s^{-1} (FWHM) wide and centered at a velocity, relative to the narrow Hβ peak, of +2280 km s^{-1}. Moreover, Wamsteker et al. show that this Hβ red shoulder varies by a factor 3 during their 1981–1984 campaign, while the blue wing remains constant within the measurement errors. This behavior suggests that, at those epochs, the variations of the blue and the red components were not in phase as happens during the 1994 campaign described in this paper (see § 5.2).

6. SUMMARY AND CONCLUSIONS

The results of optical ground-based monitoring of the high-luminosity Seyfert 1 galaxy F9 have been presented. These data were obtained in conjunction with a large *IUE* monitoring project that is described elsewhere (Paper IX). Unfortunately, the highest amplitude variations detected in the longer UV campaign are not sampled in the optical because the core of the ground-based campaign was completed before the UV increase started, and these results are thus based on a more limited time series of data characterized by lower overall variability.

1. The optical continuum (measured at an observed wavelength of 5340 Å) varied significantly during this monitoring period. The optical continuum light curve resembles that of the UV continuum, but with lower amplitude variations. After allowing for contamination of the optical light curve by starlight from the host-galaxy and Fe II emission from the BLR, we find that the amplitude of the continuum variations at 5340 Å is about the same as at 1390 Å. In contrast to what has been reported for most other sources, it appears that in F9 the continuum does not get "harder" as it gets brighter, as had been previously concluded from UV alone by Recondo-González et al. (1997) and as we reported in Paper IX.

2. Cross-correlation analysis reveals that there is no detectable (i.e., ≥1–2 day) delay between the UV and optical continuum variations, as has been found in lower luminosity AGNs.

3. Cross-correlation analysis reveals that Hβ lags behind the UV continuum by ~23 ± 3 days, rather larger than the lag found for Lyα (~15 days; Paper IX), which is reminiscent of results for lower luminosity AGNs such as NGC 4151, NGC 5548, and NGC 3783.

4. We examined the behavior of Hβ in various radial-velocity (v_r) ranges and could find no appreciable differences between the central (-5900 km s^{-1} $\leq v_r \leq +4600$ km s^{-1}), blue-side (-3200 km s^{-1} $\leq v_r \leq -400$ km s^{-1}), or red-side ($+400$ km s^{-1} $\leq v_r \leq +3200$ km s^{-1}) flux light curves, except for mild indications of larger amplitude variations of the last two features, which is attributable the dilution of the central flux by nonvariable emission features, particularly the constant Hβ narrow-line component and Fe II emission.

5. The Hβ line profile variations can be described in terms of a two-component structure, one component shifted to the blue and another one to the red of the line peak, and of similar widths (~2500 km s^{-1}). During this monitoring campaign, both components appear to vary in phase.

The results derived from this study confirm those obtained from the UV campaign (Paper IX), most importantly that F9 appears to vary on similar timescales and with comparable amplitudes as other radio-quiet AGNs of 1–2 orders of magnitude lower intrinsic luminosity, e.g., NGC 5548, NGC 3783, and NGC 4151. In fact, all these AGNs monitored by the AGN Watch consortium show variations down to the temporal sampling limit.

The absence of a detectable lag (i.e., greater than 1–2 days) between the UV and optical continuum variations places severe constraints on current models to explain the origin of the UV–optical continuum emission. In particular, for models with temperature gradients, where the radiation at any wavelength arises predominantly from a specific distance to the central black hole (such as accretion disk models), the lag of detectable UV/optical continuum lag requires the signal connecting the different parts emitting at different wavelengths propagates at speeds close to a significant fraction of the speed of light (see, e.g., Courvoisier & Clavel 1991). In such models, the distances of the different

emitting regions, and the separation between them, scale with the mass of the central object, which, in turn scale with the luminosity of the AGN. On account of the F9 luminosity, higher by $\gtrsim 1$ order of magnitude than that of NGC 5548 and NGC 3783, the absence of any measurable time delay between the UV and optical variations is more striking than in the two other sources that have been studied at similar temporal resolution (Korista et al. 1995; Reichert et al. 1994).

This campaign has also shown that variations of at least a factor of 2 on timescales of 70–90 days are superimposed on the long-term changes already known to occur in F9 (see, e.g., Clavel, Wamsteker, & Glass 1989). Therefore, the emitting region must be smaller than a few light months across, although this is not very restrictive.

The delay in the Hβ response to continuum fluctuations gives an indication of the length scale of the inner Hβ emitting region in the BLR of F9. Following the discussion on Paper IX, one can scale the NGC 5548 Hβ time delay (i.e., 20 days; Peterson et al. 1994) to the mean luminosity of F9 during this campaign (assuming the $r \propto L^{1/2}$ dependence). We obtain a value of 50 days, larger than the value of 23 ± 3 measured here, but of the same order of magnitude. For the previous AGN Watch campaigns on other Seyfert 1 galaxies, (NGC 5548 [Peterson et al. 1994] and NGC 3783 [Stirpe et al. 1994]), the results indicate an Hβ lag (20 ± 2 and 8 ± 3, respectively) twice as long as that of Lyα (11 and 4 ± 2 days, respectively). Hence, the Hβ/Lyα-lag ratio in F9 is smaller but consistent within the errors with the above results. This strongly suggests a photoionized BLR that is stratified, i.e., its physical properties range with the distance to the central source, the highest ionization lines arising in the regions which are closest to the central source.

The consistency of the Hβ/Lyα-lag ratio in F9, NGC 5548 and NGC 3783, does not help to solve the C IV λ1549 problem pointed out in Paper IX. In fact, is still puzzling that in F9, the results of Paper IX show that the C IV λ1549 response time is different from that of Lyα, while in the other well-studied AGNs, their response times are similar.

One can also briefly compare the scale length of the BLR in the radio-quiet objects already studied by the AGN Watch consortium to test whether there is a luminosity-size relationship. The inferred HB-BLR length scales are 23 ± 3 days (F9, present campaign), 20 ± 2 days (NGC 5548, during the first 3 yr of the AGN Watch monitoring; Peterson et al. 1994), 10 ± 2 days (NGC 5548, during the *HST-IUE* campaign in 1993; Korista et al. 1995) and 8 ± 3 days (NGC 3783; Stirpe et al. 1994). Assuming $H_0 = 75$ km s^{-1} Mpc^{-1}, the corresponding mean UV luminosities at $\sim$1450 Å are as follows: 3.6×10^{41} ergs s^{-1} Å^{-1}, 5.6×10^{40} ergs s^{-1} Å^{-1}, 4.4×10^{40} ergs s^{-1} Å^{-1}, and 1.9×10^{40} ergs s^{-1} Å^{-1}, respectively. The AGN Watch campaign on NGC 4151 has been successful only in setting limits to the Hβ lag to continuum variations, in between 0 and 3 days, while no lags have been determined for the C IV λ1549 line emission. The mean UV luminosity of the AGN in NGC 4151 during this campaign was 8×10^{39} ergs s^{-1} Å^{-1}. There is a clear trend for the lags to be longer as the luminosity increases, but whether this relationship follows the naive $L \propto r^{1/2}$ law should be subject of a more critical discussion is out of the scope of this paper. A discussion like this should at least take into account the uncertainties in the quoted luminosities and all the systematic errors in the line/continuum lags not considered here.

More striking is the dramatic difference between the lags obtained by Clavel et al. (1989) and Lub & de Ruiter (1992) for the previous F9 monitoring campaigns, during a factor–of 30 decrease in UV luminosity in 6 yr. The Hβ lag measured by Lub & de Ruiter was 270 ± 150 days. This is not the first time that discrepancies in emission-line lags for a single AGN are found. Evidence for a changing lag has been shown by Peterson et al. (1994) in NGC 5548. Kaspi et al. (1996), and the authors they cite, show that in NGC 4151 the Hβ lag changed from 9 ± 2 when its mean 1450 Å luminosity was $\sim 1.1 \times 10^{39}$ ergs s^{-1} Å^{-1} to 0–3 days, when its luminosity was about 8 times higher. They discuss the possibilities that the discrepancy may be related to a different variability timescale of the *ionizing* continuum, or to a real change in the BLR gas distribution in the interval between the two campaigns. However, according to Kaspi et al., in NGC 4151 the time delay and luminosity seem to be inversely correlated, which is the opposite to what has been found in F9 and NGC 5548, where the Hβ time delays are shorter when the AGN luminosity is lower. Therefore, the explanations could be different in the three cases. Possible explanations and interpretations for the F9 case are discussed in Paper IX to where the reader is referred. We only summarize here the likely possibilities discussed: (1) the two monitoring programs sampled completely different scales in a very extended BLR; (2) as a consequence of the significant change in mean luminosity, there has been a change in the optical depth in BLR clouds; and (3) there has been a significant rearrangement of the BLR gas between the two experiments.

The two-component structure of the variable Hβ profile is similar to what has been reported for UV line decomposition by Recondo-González et al. (1997), though the response of Hβ to continuum variations seems to differ. While these authors find that for the long-term, large-amplitude continuum variations, the blue component response is delayed relative to the red one, the two components of Hβ seem to vary in phase, which rules out radial motions as the main cause of the observed Hβ profile variations in 1994. However, the Hβ behavior was different during previous campaigns in 1991–1992 and in 1981–1984, when only one component (the blue and the red, respectively) showed up significant variations (Winge et al. 1996; Wamsteker et al. 1985).

The authors are grateful to all the observatories involved for the generous allocation of observing time, and to T. Storchi-Bergmann and M. G. Pastoriza, who supported the proposals but did not feel that their contribution was sufficient for them to be co-authors. CASLEO is operated under agreement between the Consejo Nacional de Investigaciones Científicas y Técnicas de la República Argentina and the National Universities of La Plata, Córdoba and San Juan, Argentina. The Porto Alegre Thompson's CCD camera is operated under a contract between UFRGS (Brazil) and CASLEO (Argentina). M. S. acknowledges partial support by Spanish CICYT grant PB-ESP95-0389-C02-02. M. D. would like to thank DFG grant SFB 328. H. D. acknowledges partial support form the Brazilian Institutions CNPq and FINEP. G. G. acknowledges a Fellowship granted by the Argentinian Institution CONICET. This work was partly supported by NSF grant AST 94-20080 to the Ohio State University.

REFERENCES

Alloin, D., Clavel, J., Peterson, B. M., Reichert, G. A., & Stirpe, G. M. 1994, in Frontiers of Space and Ground-based Astronomy, ed. W. Wamsteker, M. S. Longair, & Y. Kondo (Dordrecht: Kluwer), 423
Baribaud, T., & Alloin, D. 1990, A&A, 236, 346
Bica, E. 1988, A&A, 195, 76
Blandford, R. D., & McKee, C. F. 1982, ApJ, 255, 419
Clavel, J., Wamsteker, W., & Glass, I. S. 1989, ApJ, 337, 236
Courvoisier, T. J.-L., & Clavel, J. 1991, A&A, 248, 389
Edelson, R. A., & Krolik, J. H. 1988, ApJ, 333, 646
Gaskell, C. M., & Sparke, L. S. 1986, ApJ, 305, 175
Griersmith, D., & Visvanathan, N. 1979, A&A, 79, 329
Kaspi, S., et al. 1996, ApJ, 470, 336
Korista, K., et al. 1995, ApJS, 97, 285
Lub, J., & de Ruiter, H. R. 1992, A&A, 256, 33
Peterson, B. M. 1988, PASP, 100, 18
———. 1993, PASP, 105, 247
Peterson, B. M., et al. 1991, ApJ, 368, 119
———. 1994, ApJ, 425, 622
Peterson, B. M., et al. 1995, PASP, 107, 579
Puchnarewicz, E. M., Mason, K. O., & Carrera, F. J. 1996, MNRAS, 283, 1311
Recondo-González, M. C., et al. 1997, A&AS, 121, 461
Reichert, G., et al. 1994, ApJ, 582, 608
Rodríguez-Pascual, P. M., et al. 1997, ApJS, 110, 9 (Paper IX)
Santos-Lleó, M., et al. 1995, MNRAS, 274, 1
Stirpe, G. M., van Groningen, E., & de Bruyn, A. G. 1989, A&A, 211, 310
Stirpe, G. M., et al. 1994, ApJ, 425, 609
van Groningen, E., & Wanders, I. 1992, PASP, 104, 700
Véron-Cetty, M. P., Woltjer, L., & Roy, A. L. 1991, A&A, 246, L73
Wamsteker, W., Alloin, D., Pelat, D., & Gilmozzi, R. 1985, ApJ, 295, L33
Wanders, I., Peterson, B. M., Pogge, R. W., DeRobertis, M. M., & van Groningen, E. 1992, A&A, 266, 72
White, R. J., & Peterson, B. M. 1994, PASP, 106, 879
Whittle, M. 1985, MNRAS, 213, 1
Winge, C., Peterson, B. M., Pastoriza, M. G., & Storchi-Bergmann, T. 1996, ApJ, 469, 648